JOURNAL OF AIRCRAFT
Vol. 39, No. 6, November–December 2002

Inverse Design Method for Designing Isolated and Wing-Mounted Engine Nacelles

Roland Wilhelm*
DLR, German Aerospace Center, 38108 Braunschweig, Germany

Because of the time-consuming process of generating complex block-structured grids and because of the achieved results in the field of computational fluid dynamics methods using arbitrary grids, an inverse design system has been developed that is capable of handling flowfield calculations on arbitrary grids. The flow solver used is the DLR TAU code, a finite volume flow solver for the solution of the Reynolds averaged Navier–Stokes equations on hybrid grids. The inverse design method is based on an iterative residual-correction-type approach to generate a geometry that satisfies a user-prescribed target pressure distribution. The design method has been adapted for the design of isolated and wing-mounted engine nacelles. Results are presented for the inverse design of isolated three-dimensional nacelles and wing-mounted engine nacelles considering the pylon. The baseline aircraft is the DLR ALVAST configuration.

Nomenclature

c	=	nacelle chord length
c_p	=	pressure coefficient
K	=	transonic similarity parameter
M_∞	=	freestream Mach number
r	=	nacelle radius
U_∞	=	freestream velocity
x, y, z	=	Cartesian coordinates
α	=	angle of attack
β	=	transformation factor
Δr	=	radial geometry difference
ϵ_{fan}	=	stream tube area ratio
Θ	=	circumferential section angle
κ	=	ratio of specific heats
Φ	=	perturbation velocity potential
ϕ	=	velocity potential

Introduction

THE aerodynamic design of single aircraft components, such as wing, nacelle, and winglet, or of a complete aircraft can be done using one of the two well-known methods: optimization techniques or inverse design techniques. Optimization techniques often focus on global parameters such as total lift or drag, the object of the optimization. An object function is formulated depending on a set of design variables, for example, nacelle diameter and intake droop angle. The aim is to minimize the object by varying the defined design parameter. Depending on the optimization strategy and the number of design variables, an optimization can become very time consuming.

In contrast, inverse design methods give the opportunity to influence the local flowfield surrounding the configuration to be designed. As the name inverse indicates, these methods change the workflow direction of the typical analysis problem where a geometry is given and a flowfield solution is desired. When a user-specified surface pressure distribution (the target) is used, these methods aim at generating a geometry that satisfies this target. In the design step, inverse methods translate a surface pressure difference into a geometry difference. The design step is followed by an analysis step in which the flowfield solution of the previously designed configuration is calculated. Subsequent iterations between these two steps yield a new design solution. Obviously, this method requires some expert knowledge about the general flow regime and the flow physics. In addition, there is no guarantee that the specified pressure distribution will yield a physical solution.

A couple of inverse design methods exist in the field of aerodynamics. The method by Campbell and Smith[1] converts the surface pressure difference between the actual and the target pressure distribution into a change in surface curvature. Integrating the new curvature distribution leads to a new surface. This method has been applied to inverse designs of isolated and installed nacelles.[2–4] Malone et al.[5] use an elastic surface method to design wing and nacelle configurations. The original method, as derived by Garabedian and McFadden,[6] relates differences in surface velocities between target and actual geometry to derivatives of the surface with respect to a pseudotime and a streamwise coordinate. Thus, the surface varies in time until the surface velocity differences approach zero.

The present paper uses an inverse design method developed by Takanashi.[7] The inverse formulation of the transonic small perturbation equation is used to convert a surface pressure difference into a geometry difference. Bartelheimer[8] extended the original method to deal with transonic flows and incorporated the scheme into the block-structured DLR Euler/Navier–Stokes flow solver FLOWer.[9] The scheme is capable of designing airfoils, wings, and nacelles.[10] Fejtek et al.[11] used the same inverse design formulation but a different flow solver to design wings of complete aircraft configurations including the pylon.

The aim of this paper is to present a new inverse design system for the design of isolated and wing-mounted engine nacelles. The design step is done using the method by Bartelheimer.[8] The analysis tool for generating the flow solution is the DLR Tau code, a flow solver for the solution of the Euler/Navier–Stokes equations on arbitrary grids.

Numerical Method

The inverse design system presented in this paper links the inverse design method formerly combined with a block-structured flow solver to the unstructured DLR Tau code.[12] Thus, a higher flexibility concerning configuration changes can be achieved because the time-consuming initial grid-generation process known for block-structured grids around complex configurations can be reduced significantly. Figure 1 gives an overview of the new system. As can be seen, the design system includes four main modules: the flow solver, the solution interpolation module, the inverse design module, and the grid deformation module. The analysis step is done

Received 26 November 2001; revision received 14 May 2002; accepted for publication 15 June 2002. Copyright © 2002 by Roland Wilhelm. Published by the American Institute of Aeronautics and Astronautics, Inc., with permission. Copies of this paper may be made for personal or internal use, on condition that the copier pay the $10.00 per-copy fee to the Copyright Clearance Center, Inc., 222 Rosewood Drive, Danvers, MA 01923; include the code 0021-8669/02 $10.00 in correspondence with the CCC.

*Research Engineer, Transport Aircraft Division, Institute of Aerodynamics and Flow Technology.

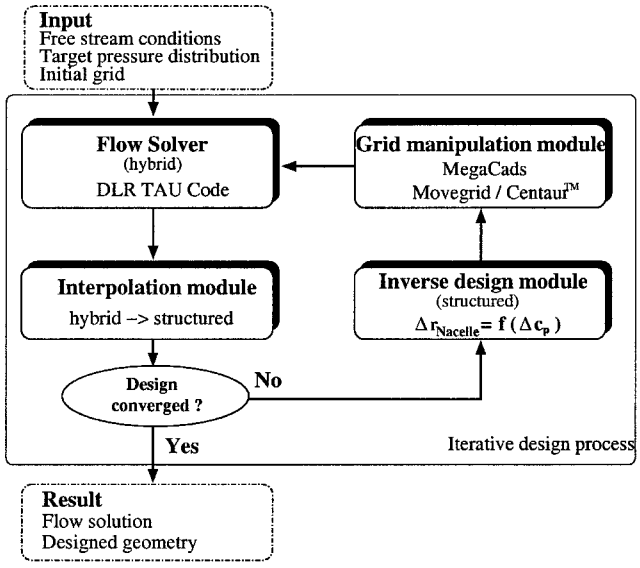

Fig. 1 Flow chart of inverse design system.

from the initial geometry and results in a flowfield solution of the actual configuration. The interpolation module transfers the necessary flowfield solution data from the surface grid consisting of triangles or quadrilaterals (depending on the surface elements used) to the design surface grid (a structured surface grid consisting of quadrilaterals). During this interpolation step, only surface pressure values on the design surface, that is, the nacelle, are taken into account because all necessary flowfield information for the design procedure is contained in these data. The design module calculates the difference between the actual and the target pressure distribution and converts it into a geometry difference. During this design step, the nacelle is treated as an isolated component without any further information from the aircraft configuration except the nacelle surface pressure. Finally, the calculated geometry difference is introduced into the finite volume grid of the last flowfield analysis to give a modified grid for the next analysis step.

The following subsections will give a detailed explanation of the conceptual and numerical methods used in the main modules flow solver, inverse design, and grid manipulation.

Flow Solver

The flow solver used within the design system is the DLR Tau code.[12] The code solves the three-dimensional Euler/Navier–Stokes equations using control volumes consisting of triangular or quadrilateral surfaces. The discretization in space is done using a central differencing scheme. Therefore, additional second- and fourth-order dissipative terms are added to the flux balance. The time integration is performed using a three-stage Runge–Kutta scheme. Acceleration techniques such as multigrid and local time stepping are applied as well. A detailed description of the flow solver including examples for validation can be found in Ref. 12.

The TAU code locates the conservative variables at the cell vertices. Therefore, a secondary grid has to be generated where each dual control volume surrounds one grid node of the primary grid. To compute the conservative variables at a grid point, the net flux of mass, momentum, and energy across the surface of the dual grid control volume has to be computed. This is done by summation of the fluxes between the actual grid node and all of its neighboring nodes. The dual grid has to be calculated using a preprocessor before the main flowfield calculation.

All calculations presented in this paper are simulated in an inviscid flow regime. Therefore, all primary grids consist of tetrahedral control volumes only. The reason for this is the time savings gained by applying the Euler instead of the Navier–Stokes equations. Especially at the beginning of a new design project, various different configurations have to be evaluated in a short time. Because for nacelle flows the main flow phenomena are sufficiently resolved in an inviscid flow regime, this simplification can be done. Nevertheless, for a final design loop, viscous flowfield calculations should be applied to resolve even the minor flow phenomena. Note that because the inverse design system handles the flow solver as a black box, this decision depends solely on the design strategy of the aerodynamicist and the time available.

The primary grids used for the flowfield calculations are generated with respect to their use in a design loop. Before the inverse design runs, the analysis grids have been evaluated in terms of number of grid points and grid density. Experimental data were used for comparison. Nevertheless, the main goal was to generate grids of high efficiency when used in a design loop while preserving the quality of the resulting flowfield calculations.

Inverse Design Module

The inverse design method presented is based on an iterative residual-correction-type approach. The residual Δc_p, that is, the pressure difference between the actual and the target pressure distribution, is used to calculate a geometry difference Δz. The correction step is done by solving an inverse formulation of the transonic small perturbation (TSP) equation as derived by Takanashi.[7]

The three-dimensional potential equation can be written in terms of a perturbation velocity potential Φ as

$$\left(1 - M_\infty^2\right)\Phi_{xx} + \Phi_{yy} + \Phi_{zz} = K \cdot \Phi_x \Phi_{xx} \qquad \text{with} \qquad K = (\kappa + 1)M_\infty^2 \tag{1}$$

where Φ is defined as

$$\phi = U_\infty(x + \Phi) \tag{2}$$

Two simplified boundary conditions can be applied to Eq. (1). The first one applies the tangency condition on the surface, whereas the second one is a simplified pressure relation

$$\Phi_z(x, y, \pm 0) = \frac{\partial z(x, y, \pm 0)}{\partial x} \tag{3}$$

$$\Phi_x(x, y, \pm 0) = -\frac{c_p(x, y, \pm 0)}{2} \tag{4}$$

The $\pm$ sign denotes the upper or lower side of the surface. To eliminate the dependency on the freestream Mach number in $\beta^2 = 1 - M_\infty^2$, a Prandtl–Glauert transformation is performed, and new coordinates $\bar{x}$, $\bar{y}$, $\bar{z}$ are introduced. When is assumed that for an initial geometry $\bar{z}(\bar{x}, \bar{y}, \pm 0)$ a flowfield solution $\bar{\Phi}(\bar{x}, \bar{y}, \bar{z})$ exists, a differential perturbation potential $\Delta\bar{\Phi}(\bar{x}, \bar{y}, \bar{z})$ can be introduced into Eq. (1):

$$\Delta\bar{\Phi}_{\bar{x}\bar{x}} + \Delta\bar{\Phi}_{\bar{y}\bar{y}} + \Delta\bar{\Phi}_{\bar{z}\bar{z}} = \frac{\partial}{\partial x}\left[\frac{1}{2}(\bar{\Phi}_{\bar{x}} + \Delta\bar{\Phi}_{\bar{x}})^2 - \frac{1}{2}(\bar{\Phi}_{\bar{x}})^2\right] \tag{5}$$

The two boundary conditions of Eqs. (3) and (4) become

$$\Delta\bar{\Phi}_{\bar{z}}(\bar{x}, \bar{y}, \pm 0) = \frac{K}{\beta^3}\frac{\partial \Delta\bar{z}(\bar{x}, \bar{y}, \pm 0)}{\partial \bar{x}} \tag{6}$$

$$\Delta\bar{\Phi}_{\bar{x}}(\bar{x}, \bar{y}, \pm 0) = -\frac{K}{2\beta^2}\Delta c_p(\bar{x}, \bar{y}, \pm 0) \tag{7}$$

The pressure difference $\Delta c_p(\bar{x}, \bar{y}, \pm 0)$ in Eq. (7) can be computed using the calculated flow solution and the prescribed target pressure distribution,

$$\Delta c_p = c_p^{\text{target}} - c_p^{\text{calculated}} \tag{8}$$

The right-hand side of Eq. (5) is known using Eqs. (4) and (7). Equation 5 can be solved for the unknown geometry difference $\bar{z}(\bar{x}, \bar{y}, \pm 0)$ using Green's theorem, as described by Bartelheimer.[8] In a final step, the computed geometry correction has to be transfered back into the original x, y, z coordinate system.

The explained solution procedure does not distinguish between flow regimes of elliptic (subsonic) or hyperbolic (supersonic) character. Therefore, the described procedure may not converge in transonic flow regions because a stable solution scheme has to use some upwind-biased formulation in hyperbolic regions to cover the correct flow physics. Bartelheimer[8] introduced a stabilizing upwind-discretization scheme into Eq. (5), which is applied in hyperbolic regions. Therefore, the modified governing design equation used is

$$\Delta\bar{\Phi}_{\bar{x}\bar{x}} + \Delta\bar{\Phi}_{\bar{y}\bar{y}} + \Delta\bar{\Phi}_{\bar{z}\bar{z}} = \frac{\partial}{\partial x}\left[\frac{1}{2}(\bar{\Phi}_{\bar{x}} + \Delta\bar{\Phi}_{\bar{x}})^2 - \frac{1}{2}(\bar{\Phi}_{\bar{x}})^2 + \Delta\bar{x}\Delta\bar{\Phi}_{\bar{x}\bar{x}}(1 - \bar{\Phi}_{\bar{x}} - \Delta\bar{\Phi}_{\bar{x}})\right] \tag{9}$$

The preceding formulas and their coordinate system are given in a general formulation applicable for wing design, that is, the x coordinate running in the streamwise direction, the y coordinate running in the spanwise direction, and the z coordinate running in the resulting direction for a right-hand side coordinate system. To use one single inverse design formulation for both wing and nacelle design, this formulation should be kept unchanged. Therefore, in the case of a nacelle design run, the coordinate system is changed, with y now being the circumferential coordinate direction and z running in the radial direction (both taken with respect to the engine axis). The x coordinate remains the streamwise direction. This partly changed coordinate system is used only for the solution of the TSP equation. In essence, for nacelle inverse design, a quasi-circular wing is formed where the inner lower wing part is not considered as part of the computational domain. The calculated geometry difference Δz, therefore, is taken as a radial geometry difference Δr. Before the calculated geometry differences are added to the actual design surface, they are smoothed in the streamwise and circumferential directions using a Bézier curve technique. Because of the structured design surface grid, the smoothing technique is applied on each constant-index grid line in both directions. Because only geometry differences are smoothed, it is necessary to start each design run with a smooth geometry that lacks any discontinuities in curvature.

As mentioned before, radial displacements of the design surface are allowed to take place in the design method. This procedure ensures that the nacelle planform remains constant throughout the whole design process. The size of the nacelle in terms of nacelle length and the thereto related intake droop angle have to be specified by the initial geometry. Two additional fixed points of the nacelle are the fan radius and the fan nozzle radius. The result of the inverse design module is a modified nacelle geometry in terms of nacelle and intake diameter whose flowfield will be analyzed in the subsequent design iteration.

To design wing-mounted nacelles, the described design concept has to be extended to compensate for the lack of surface pressure data in the pylon cutout zone. The inverse design module interpolates surface pressure data from both sides of the pylon to generate reasonable pressure values in this region. When this is done, the solution of the TSP equation is carried out as if the case would be an isolated nacelle design. The resulting isolated nacelle design surface is processed in the grid manipulation module (see next section) where it is merged with the pylon to result into a new configuration.

Because the inverse design method is employed in an iterative design loop, it can be expected that with each iteration the solution converges to a final result. Nevertheless, this assumption is only valid if the design problem is not ill posed, that is, the prescribed target pressure distribution represents a physical solution for the given global parameters. Bartelheimer[8] tested the presented design method with respect to consistency and convergence behavior. He did parameter variations for the main design parameters such as design grid density and smoothing parameters. Within this work, his findings were taken as the design guideline.

Grid Manipulation

The grid manipulation is necessary to generate a computational grid for the modified nacelle geometry. In addition to the possibility of generating the finite volume grid including the modified nacelle in each design iteration from scratch (which becomes very time consuming), the more efficient way is to apply a grid-manipulation method that fits an existing finite volume grid to a modified configuration. Also, in the case where only one finite volume grid consisting of a constant number of grid points would be used for all flowfield calculations in the design loop, the restart ability of the flow solver also contributes to the systems overall efficiency. Finally, because the grid manipulation process runs in an iterative design loop, all geometry and grid modification steps have to be done automatically, in a closed-process chain without any intermediate user input.

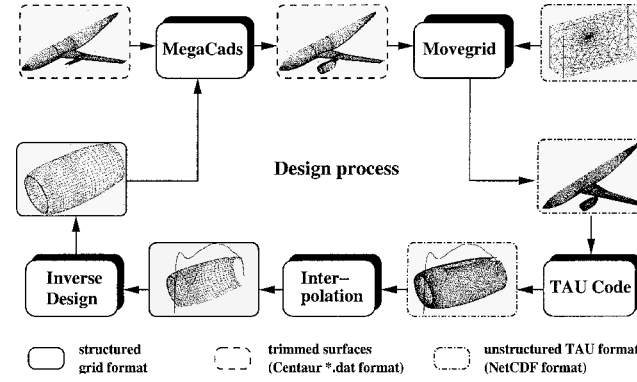

Fig. 2 Grid and geometry treatment in the inverse design system.

The grid generation package Centaur is used to generate the initial finite volume grid for the start configuration. In general, Centaur is capable of designing hybrid grids consisting of prismatic, hexahedral, pyramidal, or tetrahedral control volumes. In case of the presented inverse design system, the initial grid has to be generated before the main inverse design run can start. Because this grid will be the baseline finite volume grid for all flowfield calculations performed in the design loop, its quality should be analyzed carefully. Within the inverse design loop, the grid treatment and manipulation is done as shown in Fig. 2.

The design loop starts with a flowfield analysis of the initial geometry utilizing the DLR TAU code. (See the right-hand side of Fig. 2.) The surface pressure distribution of the nacelle is one of the results, which is transfered to the structured design surface grid via an interpolation module. The design module itself carries out an isolated nacelle design based on the actual surface pressure distribution, which may result from an isolated nacelle or a complete aircraft configuration calculation. The inverse design module performs one design step, resulting in a modified nacelle shape. In the next step, the batch version of the DLR grid generation package MegaCads[13] is used to merge the new design surface, that is, the nacelle, with the remaining aircraft components such as wing, fuselage, and pylon. In particular, because of the modified nacelle surface, a new intersection line between pylon and nacelle is calculated. To result in a water-tight domain, farfield and symmetry plane are added, too. The complete configuration is now represented by trimmed surfaces, a data format that can be read by Centaur. The Centaur package includes a grid-manipulation module *Movegrid*, which fits an existing finite volume grid to a modified configuration. The algorithm moves surface grid points located at a former position onto the new nacelle surface. After this surface point mapping, the surrounding interior field points are moved in a decaying manner, depending on their individual distance from the modified surface. Applying *Movegrid* will result in a grid that will be used for the flowfield analysis in the next design iteration.

As can bee seen, the combination of both structured and hybrid grid formats makes the inverse design system very flexible and viable. Nevertheless, care has to be taken because this grid point movement is limited to a certain extent.

Results

In the following section, results using the new inverse design system will be presented. The system has been used to design both

Table 1 Test cases for the inverse design system

Case	Target	Design	M_∞	α, deg	ϵ_{fan}
1	VHBR (isolated nacelle)	Redesign	0.75	2.0	0.96
2	Hybrid-laminar flow nacelle	Design	0.82	2.0	0.96
3	ALVAST-VHBR (installed nacelle)	Redesign	0.75	1.15	0.96
4	ALVAST-VHBR (target from $M_\infty = 0.75$)	Design	0.82	1.15	0.96

isolated and installed (wing-mounted) nacelles at different cruise conditions. Table 1 summarizes the calculations.

In general, the test cases shown consist of redesign and design cases, that is, cases where the solution is known in advance (redesign) and others where it is unknown (design). For redesign cases, the target pressure distribution is gained by an analysis calculation of the final geometry. When generating a target pressure distribution for a pure design case, various constraints have to be taken into account. The nacelle trailing-edge Mach number is determined by the fan exhaust nozzle system. The intake fan Mach number is fixed by the stream tube area ratio ϵ_{fan} (if isentropic flow is assumed), which is the area ratio between the intake stream tube at infinity and at the fan face. The position of the stagnation point depends on the angle of attack and also on the stream tube area ratio. Therefore, rather than generating a target pressure distribution from scratch without any knowledge of the flowfield, it is better to generate a start solution and modify it according to the design goal.

Case 1

The first test case is the redesign of an existing isolated nacelle. This test strategy ensures that no unphysical target pressure distribution, a so-called ill-posed problem, is prescribed. The already known geometry to be designed is a typical nonaxi-symmetric very high bypass ratio (VHBR) turbofan nacelle with an intake droop angle of 5 deg. The initial geometry is a nacelle of the same planform as the target. Its shape is constructed out of the scaled profiles of the target nacelle at 90 deg (horizontal plane) only. In essence, when the intake droop angle was neglected, the initial nacelle would be axisymmetric. The freestream Mach number is $M_\infty = 0.75$, and the angle of attack is $\alpha = 2.0$ deg. As mentioned before, the calculation is done in an inviscid flow regime. The intake mass flow is specified using a value of $\epsilon_{\text{fan}} = 0.96$ for the stream tube area ratio. Because no yaw angle is taken into account, a vertical symmetry plane is used to calculate only one-half of the nacelle's flowfield.

Figure 3 shows the dimensionless surface pressure coefficient c_p over the dimensionless local nacelle chord length x/c at three circumferential sections ($\theta = 0$, 90, and 180 deg). Also shown are the nacelle profiles of the corresponding sections. As can be seen, the target pressure distribution is met by the designed nacelle geometry in all three sections. The difference in the pressure distributions at $\theta = 90$ deg between the initial and final data is due to three-dimensional effects of the flowfield. As a reminder, the $\theta = 90$ deg nacelle section should be kept constant during the design run. In Fig. 3, the pressure distributions show some minor oscillations on the outer nacelle from the leading edge up to $x/c = 0.15$. An analysis of the surface curvature distribution in three circumferential sections shown in Fig. 4 shows that the curvature is not smooth in this region. A comparison with the intake region indicates that this unsmooth contour is the reason for the pressure oscillations. Although the inverse design system matches the target pressure distribution in this region quite well, it neither matches the prescribed values exactly nor does it eliminate the unsmooth contour. This is an example for the inability of the inverse design system to smooth initial geometries, as already mentioned in the "Inverse Design Module" section. The convergence protocol of this redesign run is shown in Fig. 5. In Fig. 5a the normalized average density residual can be seen. The first 1100 time steps are related to the analysis calculation of the initial geometry. Throughout the following time steps, every single flowfield calculation of the inverse design loop results in a converged solution. Also, with an increasing number of design cycles, the top level of the density residual decreases because the

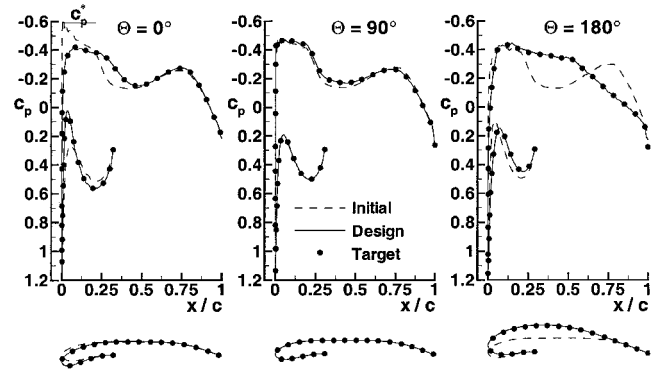

Fig. 3 Redesign of an isolated nacelle: surface pressure distributions and nacelle profiles in three circumferential sections.

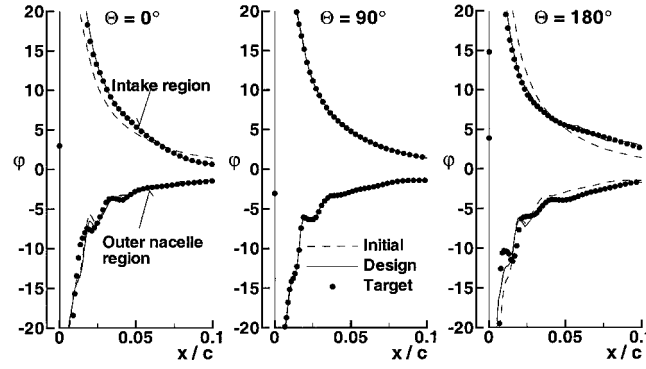

Fig. 4 Redesign of an isolated nacelle: surface curvature distribution in three circumferential sections.

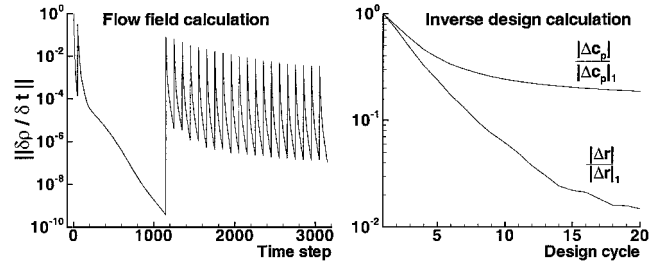

a) b)

Fig. 5 Redesign of an isolated nacelle: a) convergence protocol including density residual and b) normalized average pressure difference and geometry change.

design approaches the geometric target solution. Figure 5b shows the normalized average pressure difference $|\overline{\Delta c_p}|$ and the normalized average geometry difference $|\overline{\Delta r}|$. Both values decrease during the design process, that is, the design solution converges to a final result.

For an indication of the quality of the grid-manipulation module, refer to Fig. 6. Shown is the upper nacelle leading edge in the vertical symmetry plane of the tetrahedral grid of both the initial and the final configuration. As can be seen, close to the nacelle surface, the surface triangles of the control volumes are identical. Close to the nacelle surface, the control volumes are rigidly moved to preserve the initial spacing. Some distance away from the surface, a transient zone exists where the modified geometry is merged into the surrounding control volumes.

Case 2

In a next test case, a target pressure distribution is prescribed for an unknown geometry. The aim is to design a typical hybrid-laminar flow nacelle at a higher freestream Mach number, that is, at $M_\infty = 0.82$, than in the redesign case 1. The angle of attack is $\alpha = 2.0$ deg. In general, hybrid-laminar flow is established by both boundary layer suction (up to a nacelle chord length of $x/c \approx 0.20$) and contouring of the nacelle. A typical resulting pressure distribution shows two acceleration peaks in the nose and midchord nacelle region. As the initial geometry, the conventional VHBR engine nacelle designed for a freestream Mach number of $M_\infty = 0.75$ is chosen. The result of this isolated nacelle design can be seen in Figs. 7 and 8. Figure 7 shows surface pressure distributions and nacelle profiles for three circumferential sections. In Fig. 8, shaded surfaces of the initial and designed nacelle in top and side view are displayed. Again the prescribed target pressure distribution is matched by the designed nacelle with good agreement. Some minor deviations from the target occur in the leading-edge region of the nacelle, especially at $\theta = 180$ deg. The prescribed higher surface pressure value is not precisely met. One possible reason is the unsteady curvature distribution of the initial VHBR nacelle, as already shown in Fig. 4. Because of the higher surface velocities in the nacelle leading-edge region compared to case 1 (close to sonic), an unsmooth surface curvature produces oscillations in the flowfield that can jeopardize the inverse design run. Nevertheless, over a wide region of the nacelle, the designed geometry fulfills the target.

Because of the second acceleration peak in all three circumferential sections, the maximum nacelle diameter is significantly increased to enhance the necessary pressure gradient. The major nacelle diameter increase occurs in the horizontal nacelle section ($\theta = 90$ deg), where the initial nacelle has been of straight cylindrical type. Note that due to the inviscid flow regime it is not possible to evaluate if the boundary layer is really laminar. The term hybrid-laminar flow nacelle, therefore, refers only to the type of target pressure distribution. The general aim of this calculation is to demonstrate the principle capability of the inverse design system to generate an a priori unknown nacelle shape.

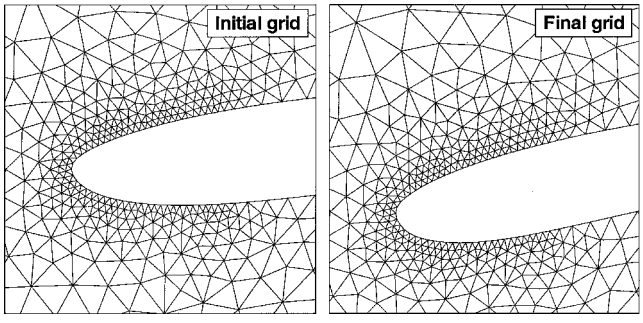

Fig. 6 Redesign of an isolated nacelle: initial and final tetrahedral grid after grid movement in the vertical symmetry plane.

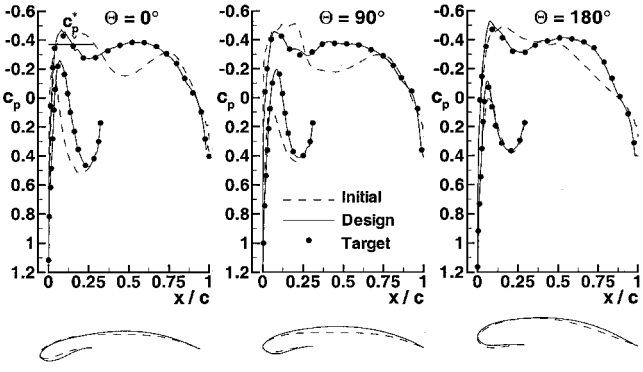

Fig. 7 Design of an isolated nacelle: surface pressure distributions and nacelle profiles in three circumferential sections.

Case 3

Besides the aim of the aerodynamicist to design single aircraft components such as an isolated nacelle, there is the even more complex task to develop and optimize installed components taking into account the complete aircraft. The design system presented in this paper is capable of performing an inverse design of an installed nacelle considerating the pylon. The next example will demonstrate this. The aircraft used for the inverse design of an installed nacelle is the DLR ALVAST configuration,[14] a generic twin engine subsonic Airbus A320-like transport aircraft. For this case, the model is equipped with the original VHBR engine nacelle. The engine is installed under a toe-in angle of 1 deg and a nose-up angle of 1.8 deg. Figure 9 gives an overview of the ALVAST configuration. To test the design system, a redesign is done again. As in the case of the isolated nacelle, the initial nacelle geometry is set up by the scaled profiles of the side section only ($\theta = 90$ deg). The prescribed nacelle target pressure distribution corresponds to the surface pressure distribution of the installed VHBR nacelle. The freestream

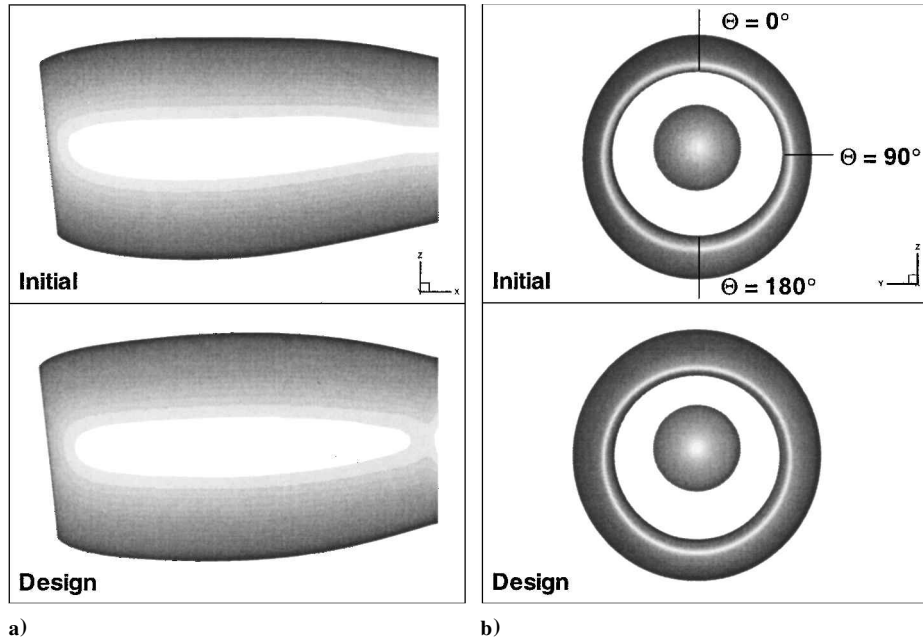

a) b)

Fig. 8 Design of an isolated nacelle: shaded a) side and b) front views of initial nacelle and designed nacelle.

and main engine parameters for the installed nacelle case are the Mach number $M_\infty = 0.75$, the angle of attack $\alpha = 1.15$ deg, and the stream tube area ratio $\epsilon_{fan} = 0.96$. Figure 10 shows surface pressure distributions and nacelle profiles in three circumferential sections: $\theta = 45$, 180, and 315 deg, (see Fig. 11 for the section location). As can be seen, the prescribed pressure distributions are met in all three sections. Figure 11 shows shaded views of the initial and designed nacelle surface. The thickness in the bottom part of the nacelle has considerably increased. Also the intake throat moved down to get into alignment with the incoming flowfield. Figure 12 shows a detail of the region where pylon and nacelle intersect. In each design cycle, the intersection line between pylon and nacelle is calculated to match the new nacelle surface. When the initial and final grids are compared in this region, the nacelles surface movement relative to the pylon is clearly visible.

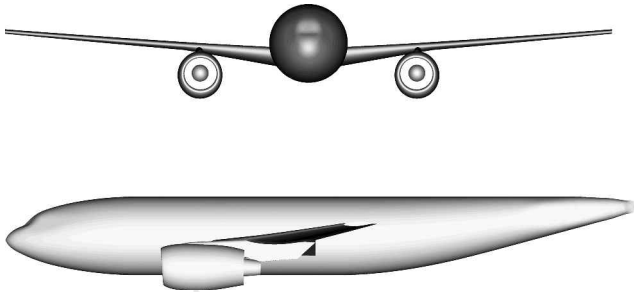

Fig. 9 DLR ALVAST-VHBR configuration.

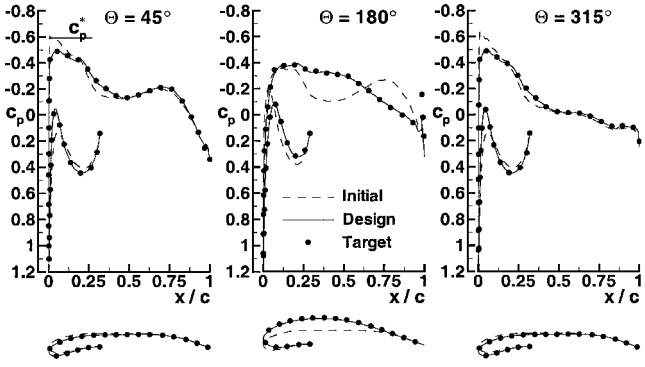

Fig. 10 Redesign of an installed nacelle: surface pressure distributions and nacelle profiles in three circumferential sections.

Case 4

In the final example, the inverse design system is tested for the design of an unknown nacelle geometry. As before, the DLR ALVAST configuration including a VHBR nacelle is considered as the initial aircraft configuration. The aim of this test case is to design a nacelle for the ALVAST configuration at a higher freestream Mach number without changing the nacelles surrounding flowfield. In other words, the increased aircraft speed should not produce any unfavorable flowfield in the vicinity of the nacelle and should, therefore, leave the nacelle flowfield unchanged. The higher freestream Mach number is $M_\infty = 0.82$, and the angle of attack is $\alpha = 1.15$ deg. The target pressure distribution is taken from the initial flowfield solution at $M_\infty = 0.75$. This example uses and ill-posed target pressure distribution. Because of the higher freestream Mach number in the actual flowfield, the prescribed target pressure value in the stagnation point can not be fulfilled by the design. Figure 13 shows the resulting surface pressure distributions and nacelle cross sections in three circumferential sections: $\theta = 45$, 180, and 315 deg (see Fig. 11 for the section location). Because of the higher freestream Mach number, the flowfield is accelerated on the outer initial nacelle surface. To meet the prescribed target pressure level resulting from the lower freestream Mach number, a slimmer nacelle with a smaller maximum nacelle diameter is designed. As can be seen, the prescribed target pressure distribution is met. Some deviations between design and target pressure distribution occur in the vicinity

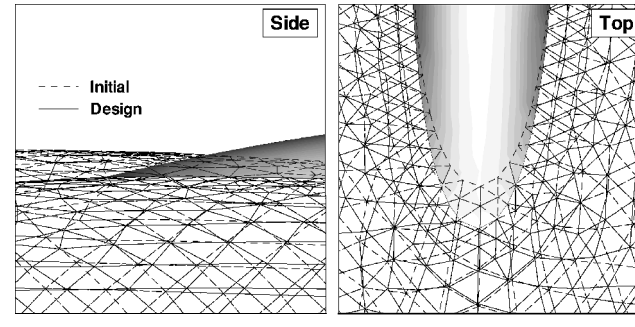

Fig. 12 Redesign of an installed nacelle: side and top view of pylon region with initial and final surface mesh.

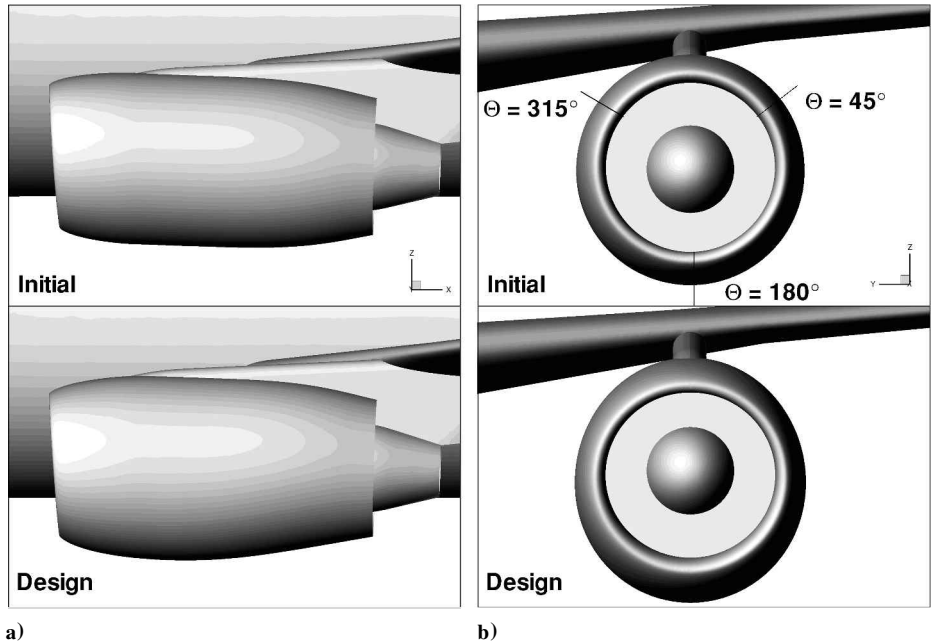

a) b)

Fig. 11 Redesign of an installed nacelle: shaded a) side and b) front views of initial nacelle and designed nacelle.

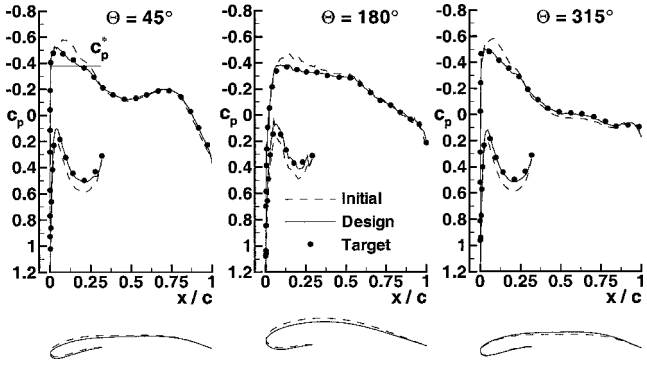

Fig. 13 Design of an installed nacelle: surface pressure distributions and nacelle profiles in three circumferential sections.

of the leading edge due to the ill-posed character of this problem and the earlier mentioned unsmooth curvature distribution. The higher pressure level in the intake region is compensated by decreasing the intake diameter and, therefore, accelerating the flowfield.

Conclusions

An algorithm for the iterative inverse design of isolated and wing-mounted engine nacelles has been presented. The method uses a residual-correction-type approach to design a nacelle surface that fulfills a prescribed target pressure distribution. The presented inverse design system uses the DLR flow solver TAU for the flowfield analysis on arbitrary grids. The geometric surface preprocessing is done using the DLR grid generation package MegaCads. Because of the modular setup of the inverse design system, it is possible to include the commercial grid-generation and modification package Centaur as a grid-deformation tool into the design loop.

The results presented show that the method is capable of designing engine nacelles. A redesign test case demonstrates the complete design functionality for isolated engine nacelles. A hybrid-laminar flow nacelle design shows an application without an a priori known solution. In addition, both redesign and design cases are presented for the design of wing-mounted engine nacelles. The results of these calculations show that the inverse design system is able to perform different design tasks even in the vicinity and while considering the pylon.

The presented test cases show that the inverse design system can be used to modify the flowfield around engine nacelles according to the user-specified pressure distribution. Nevertheless, the generation of these pressure distributions still requires some expert knowledge in the field of aerodynamics.

Future work should focus on the further development of the inverse design system because the interaction between different aircraft components such as wing, pylon, or nacelle can be taken into account during the design process. One future application can be a wing inverse design under the influence of the pylon and nacelle.

Acknowledgments

The work presented resulted from a joint partnership between Rolls–Royce, Germany and the DLR, Institute of Aerodynamics and Flow Technology, Braunschweig, Germany. The author wishes to thank both organizations for their advice and support. Also, special thanks go to H. McMorris of CentaurSoft for his help and support.

References

[1]Campbell, R. L., and Smith, L. A., "A Hybrid Algorithm for Transonic Airfoil and Wing Design," AIAA Paper 87-2552, 1987.

[2]Bell, R. A., and Cedar, R. D., "An Inverse Method for the Aerodynamic Design of Three-Dimensional Aircraft Engine Nacelles," *3rd International Conference on Inverse Design Concepts and Optimization in Engineering Sciences*, edited by G. S. Dulikravich, NTIS, Washington, DC, 1991, pp. 405–417.

[3]Chen, H. C., "An Installed Nacelle Design Method Using Multiblock Euler Solver," AIAA Paper 93-0528, 1993.

[4]Lin, W. F., Chen, A. W., and Tinoco, E. N., "3D Transonic Nacelle and Winglet Design," AIAA Paper 90-3064, 1990.

[5]Malone, J. B., Vadyak, J., and Sankar, L. N., "A Technique for the Inverse Aerodynamic Design of Nacelles and Wing Configurations," AIAA Paper 85-4096, 1985.

[6]Garabedian, P., and McFadden, G., "Design of Supercritical Swept Wings," *AIAA Journal*, Vol. 20, No. 3, 1982, pp. 289–291.

[7]Takanashi, S., "Iterative Three-Dimensional Transonic Wing Design Using Integral Equations," *Journal of Aircraft*, Vol. 22, No. 8, 1985, pp. 655–660.

[8]Bartelheimer, W., "An Improved Integral Equation Method for the Design of Transonic Airfoils and Wings," AIAA Paper 95-1688, 1995.

[9]Kroll, N., Radespiel, R., and Rossow, C.-C., "Accurate and Efficient Flow Solvers for 3D Applications on Structured Meshes," Rept. R-807, AGARD, 1995, pp. 4.1–4.59.

[10]Hepperle, M., Bartelheimer, W., and Bousquet, O., "Application of an Inverse Design Method to the Design of Transonic Nacelles," *Proceedings of the Workshop on Aspects of Engine-Airframe Integration for Transport Aircraft*, edited by H. Hoheisel, DLR, Braunschweig, Germany, 1996, pp. 13.1–13.14.

[11]Fejtek, I., Jones, D., Waller, G., Hansen, E., and Obayashi, S., "A Transonic Wing Inverse Design Capability for Complete Aircraft Configurations," AIAA Paper 2001-2443, 2001.

[12]Gerhold, T., Friedrich, O., Evans, J., and Galle, M., "Calculation of Complex Three-Dimensional Configurations Employing the DLR TAU-Code," AIAA Paper 97-0167, 1997.

[13]Brodersen, O., Hepperle, M., Ronzheimer, A., Rossow, C.-C., and Schöning, B., "The Parametric Grid Generation System MegaCads," *5th International Conference on Numerical Grid Generation in Computational Fluid Dynamics and Related Fields*, edited by B. K. Soni, J. F. Thompson, J. Häuser and P. Eisenmann, ISGG, Mississippi State Univ., 1996, pp. 353–362.

[14]Kiock, R., "The ALVAST Model of DLR," DLR Institutsbericht 129-96/22, DLR, German Aerospace Research Center, Braunschweig, Germany, Oct. 1996.